Terrestrial gamma ray flashes and lightning discharges

U. S. Inan,[1] M. B. Cohen,[1] R. K. Said,[1] D. M. Smith,[2] and L. I. Lopez[3]

Received 2 June 2006; revised 14 July 2006; accepted 31 July 2006; published 19 September 2006.

[1] Analysis of ELF/VLF broadband data from Palmer Station, Antarctica indicates that 76% Terrestrial Gamma-ray Flashes (TGFs) detected on the RHESSI spacecraft occur in association with lightning-generated radio atmospherics arriving from near the footprint of RHESSI and within a few ms of the TGF. The remaining TGFs are not associated with any radio atmospheric, thus by implication CG lightning. The peak currents of TGF-associated lightning discharges are often among the most intense from a given storm, with the degree of this association apparently varying between oceanic and land regions. The time-integrated ELF energy of the associated sferics (and thus the lightning charge moment) exhibit much less tendency to be large. Statistical analysis of the spread in arrival time suggests a ~2 ms variance due to factors other than geometry and measurement error. **Citation:** Inan, U. S., M. B. Cohen, R. K. Said, D. M. Smith, and L. I. Lopez (2006), Terrestrial gamma ray flashes and lightning discharges, *Geophys. Res. Lett.*, *33*, L18802, doi:10.1029/2006GL027085.

1. Introduction

[2] TGFs were first observed in the early 1990s by the Compton Gamma Ray Observatory (CGRO) [*Fishman et al.*, 1994], and subsequently linked to lightning discharges [*Inan et al.*, 1996] [also *Cohen et al.*, 2006]. More recently, the Reuven Ramaty High Energy Solar Spectroscopic Imager (RHESSI) spacecraft [*Smith et al.*, 2005], observed ~13 TGFs per month, establishing a global occurrence rate of ~50 per day, due to its continuous data acquisition with no trigger threshold. TGFs are believed produced by bremsstrahlung radiation from relativistic electrons accelerated above thunderstorms. Suggested mechanisms include relativistic runaway breakdown from quasi-static (QES) electric fields at >30 km [*Lehtinen et al.*, 1999; *Roussel-Dupre et al.*, 1998], low altitude (<20 km) QES-driven runaway electrons [*Gurevich et al.*, 2004], and heating by the fast moving electromagnetic pulse (EMP) associated with of CG lightning [*Inan and Lehtinen*, 2005].

[3] Cloud-to-ground (CG) lightning discharges radiate a large fraction of their electromagnetic energy between 30 Hz–30 kHz [*Uman*, 1987, p. 119]. This energy is efficiently guided by the Earth-ionosphere waveguide, and propagates at a velocity close to the speed of light, with typical attenuation rates of only a few dB per Megameter [*Davies*, 1990; p. 389]. These so-called radio atmospherics (or sferics) can be detected from global distances.

2. Data and Methodology

[4] ELF/VLF recordings made at Palmer Station, Antarctica consist of wideband (100 Hz to 50 kHz) waveforms of electromagnetic fields measured with two orthogonal wire-loop air-core antennas, oriented in the geographic North-South (N/S) and East-West (E/W) directions. For sferics arriving over distances of ~10 Mm, the arrival azimuth can be determined with ~1–2° accuracy [*Wood and Inan*, 2004]. The timing standard for Palmer ELF/VLF recordings is a 100 kHz GPS derived timing signal, providing inherent accuracy of ~100 ns. ELF/VLF data of this type is used for estimating the geolocation and timing of lightning flashes [*Wood and Inan*, 2004], as well as properties of the lightning strike like charge moment [*Cummer and Inan*, 1997] and peak current [*Reising et al.*, 1996; *Wood*, 2005].

[5] The RHESSI satellite is a NASA Small Explorer mission designed to study hard X-rays and gamma rays from solar flares. Its nine germanium detectors are enclosed in a lightweight aluminum cryostat, and are sensitive to penetrating radiation from any direction. They typically register 20 to 40 counts for each TGF; the average TGF duration is 0.7 ms. No direction information is available, but luminosity arguments suggest that most TGFs occur within 100's of km of the nadir point [*Smith et al.*, 2005], in agreement with subsequent ground measurements [*Cummer et al.*, 2005]. RHESSI's absolute timing is currently uncertain to 2–3 ms.

[6] The VLF intensity of a sferic is measured by taking the peak magnetic field in the range 5.5 kHz–11 kHz (extended from *Reising et al.* [1996]). The VLF frequencies of sferics are dominated by low order qTE and qTM Earth-ionosphere waveguide modes, traveling approximately at *c*. The peak VLF intensity is closely related to the peak current of the lightning discharge [*Reising et al.*, 1996], as recorded (for example) by the National Lightning Detection Network (NLDN) [*Cummins et al.*, 1998]. The ELF energy content of a sferic has been defined as the average intensity below 1.0 kHz for a 10 ms period [*Reising et al.*, 1996]. Since Palmer data was recorded after high-pass filtering, we use the range 150 Hz–1.5 kHz, and integrate over 8 ms. The upper cutoff of 1.5 kHz is below the first order waveguide cutoff frequencies, so that only the wave energy propagating in the qTEM mode is represented. The ELF energy is closely linked to the lightning total charge moment [*Cummer and Inan*, 1997], though in practice charge moment is difficult to measure remotely and reliably.

[1]STAR Laboratory, Electrical Engineering Department, Stanford University, Stanford, California, USA.
[2]Institute for Particle Physics, University of California, Santa Cruz, California, USA.
[3]Department of Physics and Astronomy, San Francisco State University, San Francisco, California, USA.

0094-8276/06/2006GL027085$05.00

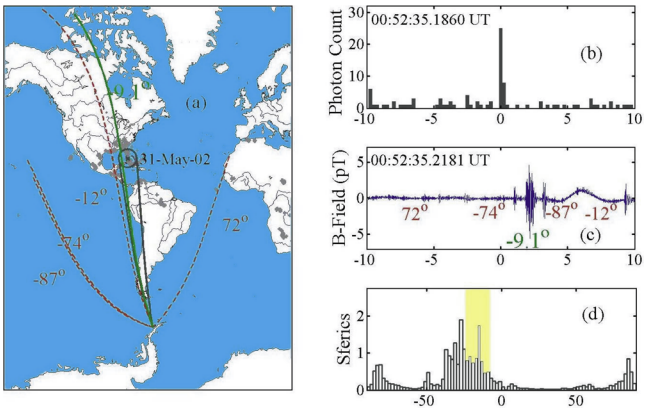

Figure 1. Methodology of associating TGFs and sferics. (a) Map with location and propagation paths of RHESSI and 600 km footprint, which is in region II. Solid line shows azimuth of TGF-associated sferic. Dashed lines indicate paths of other sferics within the 20 ms window. 12-hour LIS data shown with grey dots. (b) RHESSI data for this TGF, 0.25 ms bins, in ms with respect to the indicated time. (c) VLF data for a 20 ms period around the indicated time-zero with arrival azimuths indicated. (d) Azimuth histogram of sferics (per second-degree), logarithmic scale, over a 30-minute span, with azimuths associated with 600 km shaded.

[7] The presence of a sferic is determined by observation of a characteristic impulsive peak in the magnetic field intensity, which is highly correlated (coefficients up to 0.95) to peak current [*Wood*, 2005] using NLDN data from a given storm. A given threshold of peak magnetic field intensity hence represents a CG peak current at a given distance [*Wood and Inan*, 2004]. The Stanford ELF/VLF system can detect impulsive sferic events above the local atmospheric noise level of ~0.1 pT, corresponding (for these TGF distances) to 1–2 kA. For the sake of conservatively accounting for possible ionospheric disturbances and other variations, we adopt a threshold of 3 kA. Thus, sferics from CG lightning above 3 kA would be observable at Palmer Station upon visual inspection of ELF/VLF waveforms. Unfortunately, no similar threshold can be established for IC lightning. However, *Wood and Inan* [2004] found that three times more sferics were observed at Palmer than recorded by NLDN for a certain storm (NLDN does not record ICs), the same as the expected ratio of ICs to CGs for the storm, which is strong evidence that a large fraction of IC strokes produce sferics detectable at Palmer Station.

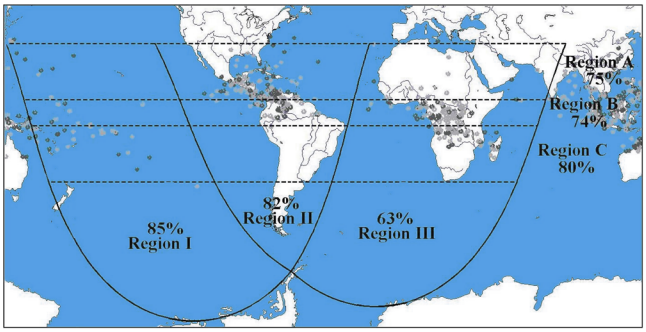

Figure 2. Reported RHESSI TGFs, Mar-02 through Jun-05. Grey indicates cases with no Palmer data, black indicates cases with available data. Division of available cases into regions. Percentages indicate fraction of cases for which associated radio atmospherics are found.

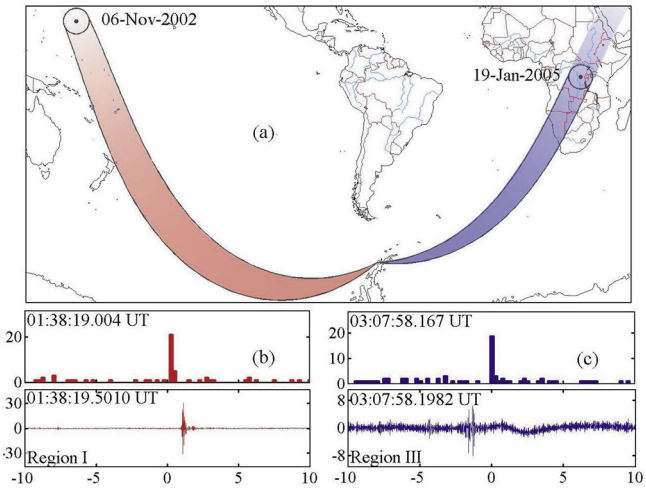

Figure 3. Global reach of sferic detection at Palmer. (a) Map showing locations of two TGFs in Regions I and III, and the great circle propagation paths to Palmer. (b)–(c) RHESSI (top) and Palmer (bot) data for the two events, same format as Figure 1b and 1c.

[8] Figure 1 shows an example of a TGF observed on RHESSI during a pass over the Caribbean Sea, together with the time-associated radio atmospheric (the third of four sferics) observed at Palmer Station. For each TGF event, we account for both the propagation time from TGF source to RHESSI, and from sferic source to Palmer, to determine 'time-zero', defined as the time a sferic would arrive at Palmer Station, *if* the TGF and the sferic occurred at the same time, directly beneath the spacecraft, at some altitude below ~60 km. The 20 ms window shown is centered around 'time-zero'. The identified sferic is one of four in this time-window. However, as is typical of most cases, it is the *only* one arriving from within ±7° of the RHESSI-azimuth within 20-ms, strongly indicative of the association between the sferic and the TGF. For most of these cases, the probability of chance occurrence of such a sferic is <2%. The arrival azimuth histogram in Figure 1 shows the detection at Palmer of sferics arriving from several active storms during the 30-min period surrounding the event, with the thunderstorm immediately below RHESSI clearly evident as a peak within the shaded region. Data from the Lightning-Imaging Sensor (LIS) on the TRMM satellite (Figure 1) is also consistent with the presence of active thunderstorms below RHESSI.

3. Observations

[9] Figure 2 shows the nadir-footprints for the 531 reported TGFs from March 2002 through June 2005, 195 of which (marked in dark circles) had Palmer data serendipitously available. We consider three broad geographic regions, Pacific (mostly ocean), Central America (ocean and land), and Africa (mostly land), referred to as Regions I, II, and III, and encompassing 116 of the 195

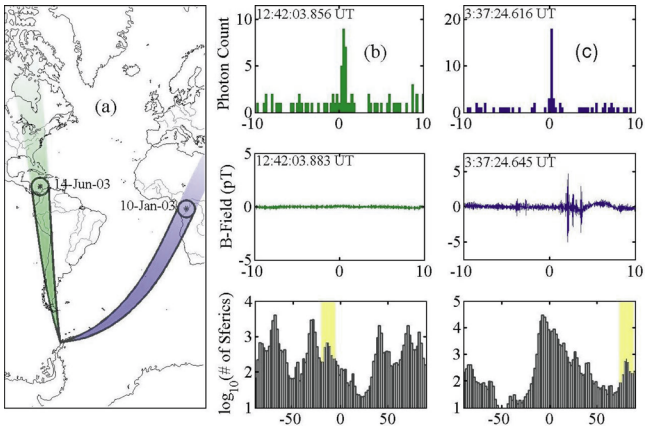

Figure 4. Two TGFs with no sferic. (a) Map showing locations of an event from regions II and III. (b)–(c) RHESSI (top), Palmer (mid), and histogram (bot) data.

events. The great circle paths to Palmer for the remaining events, in South/East Asia and Australia, pass over the Antarctic polar cap, resulting in high attenuation due to lossy ice and the auroral ionosphere [*Westerlund and Reder*, 1973]. In addition, TGFs are divided by latitude, in such a way as to place 1/3 of the total cases in the equatorial region, with the rest divided between northern and southern regions (dividing lines ~7° latitude), referred to as Regions A, B, and C. Figure 3 shows three TGF events detected by RHESSI. As before, only one radio atmospheric arrives from within ±7° and ±3 ms of the RHESSI-azimuth and time-zero, respectively, within the 20-ms windows. Of the 116 cases considered, similar associated sferics were found for 88 (76%). Sferics were found for 17/20 events (85%) in Region I, 45/55 events (82%) in Region II, and 26/41 events (63%) in Region III, as shown in Figure 3. Regions A, B, and C had very similar fractions, indicating that sferic propagation distance is not a significant factor.

[10] Figure 4 shows two TGF events with no associated sferic. An active thunderstorm is clearly evident in the direction of the RHESSI-footprint, producing ~1.8 and ~1.4 sferics per second for the Region II and III examples, respectively. The Region II example shows complete lack of any sferics (even small) during this 20-ms window, and the sferics for the Region III example are unambiguously determined to have arrived from other regions. We can safely conclude that these particular TGFs occur without any accompanying CG lightning of >3 kA peak intensity. Furthermore, these TGFs likely occur without accompanying lightning of any type within the 20 ms period. For all TGFs without an associated sferic, the geomagnetically conjugate region of RHESSI is checked for sferics, accounting for interhemispheric propagation time of electrons in accordance with conjugate effects predicted by *Lehtinen et al.* [2001]. No convincing evidence of a conjugate TGF source is found.

[11] To describe the peak-VLF and time-integrated ELF intensities of TGF-associated lightning, we compare TGF-associated sferics with others arriving from the same region (i.e., the nominal 600-km radius RHESSI footprint region) during the 30-min period surrounding the TGF. Only sferics above a certain signal/noise threshold were chosen (within ~10 dB of the noise floor), so as to eliminate those whose parameters cannot be accurately estimated. Figure 5 shows histograms, by Region, of the peak-VLF and time-integrated ELF intensities of the causative sferics, in terms of their percentile group. For example, 10 of 17 Region I cases have peak-VLF intensities in the strongest 20%.

[12] The results indicate a clear trend for TGF-associated sferics to have particularly high peak-VLF intensities (and therefore, for the causative strokes to have high peak current), consistent with TGF-production via runaway acceleration by lightning-EMP fields [*Inan and Lehtinen*, 2005]. However, some TGFs occur in association with sferics of relatively small peak-VLF intensities, possibly corresponding to strong IC lightning strokes.

[13] The selectivity toward peak-VLF intensity apparently varies by region. It is strongest in the mostly oceanic Region I, somewhat less apparent for the mixedland/ocean Region III, and significantly less apparent for the mostly land Region III. This may indicate differing conditions for TGF production between land and ocean locations. When broken up by latitudinal region, the VLF selectivity is weaker for Region B, possibly indicating that TGFs are easier to generate or detect near the equator. However, this may be a byproduct of the variation in selectivity between Regions I-III, since the three clusters of TGFs have different latitude centers.

[14] The histogram of time-integrated ELF intensities is much less suggestive of selectivity, in all regions. This measurement is complicated by the occurrence of other sferics within 8-ms, signal-to-noise ratio throughout the integration window, and higher attenuation rate of the ELF content, whereas the peak-VLF intensity measurement is more robust since the peak intensity is typically >40 dB above the noise floor. Nevertheless, Figure 5 indicates that TGF production is not dependent upon the presence of continuing currents and (by implication) unusually large amounts of charge transfer, in agreement with more direct measurements of charge removal using a few TGF-associated sferics observed at close range [*Cummer et*

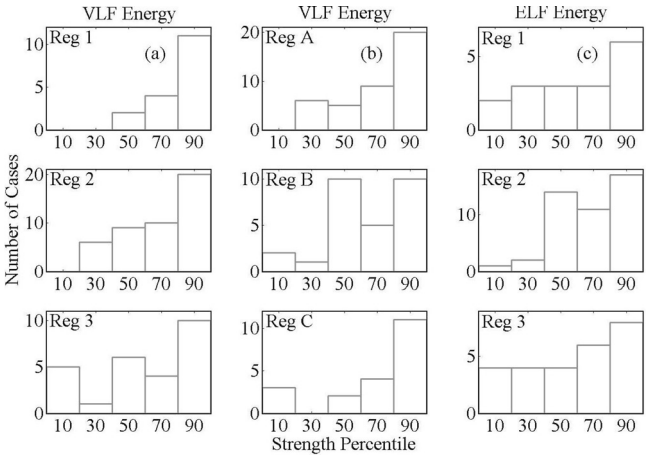

Figure 5. VLF and ELF intensities of associated sferics. (a) All matching sferics are given a VLF intensity percentile compared to all other sferics from similar direction over 30 minutes. Separated by Regions I, II, III, 88 total cases. (b) Same, but divided by Region A, B, C. (c) Regions I–III by ELF intensity.

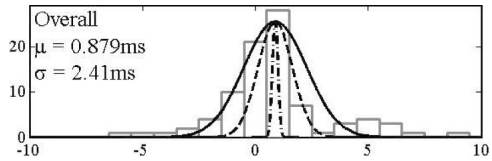

Figure 6. Arrival times of matching sferics. Positive numbers indicate late arriving sferics, or earlier occurring TGFs. Black curve shows best fit Gaussian. Dashed curves show the shape of distributions due strictly to geometry, assuming detection radius of 600 km (middle curve) and 300 km (inner curve).

al., 2005]. Overall, the lack of ELF intensity selectivity indicates that intense QE fields at high altitudes [*Lehtinen et al.*, 1999; *Roussel-Dupre et al.*, 1998] are not likely to be the drivers for at least a large fraction of RHESSI TGFs.

[15] We do not know whether the identified sferic is the only one from the thunderstorm that could have produced TGFs. For example, in the case shown in Figure 1, a sferic arriving from within ±1° of the TGF-associated sferic, and having ± 50% larger VLF peak intensity, occurred just ±30 ms later, with no TGF being reported on RHESSI. RHESSI rarely detects multiple TGFs in the same pass over a thunderstorm. Only one instance had available Palmer data, on May 4, 2002 over Africa, with 15 seconds between two TGFs. ELF/VLF analysis showed an associated radio atmospheric for the second TGF, but not the first.

[16] The sferic arrival time at Palmer may vary from the calculated time-zero due to the TGF occurring at some distance from the RHESSI-nadir point, the TGF being before or after the lightning discharge, or measurement uncertainties. The observed distribution of arrival times with respect to time-zero is shown in Figure 6.

[17] The variance in arrival time can occur due to geometry (σ^2_{GEO}), errors in TGF or VLF measurements (σ^2_{VLF} and σ^2_{TGF}), as well as the physical process(es) underlying TGFs, or other unaccounted for factors (i.e. a remainder of σ^2_{REM}). These uncertainties are independent, and so their respective variances are additive. For σ^2_{GEO}, we assume a Gaussian distribution of TGF locations with respect to RHESSI-nadir. For full-width radius 300 km (standard deviation 150 km) sferic arrival times at Palmer would be Gaussian with mean of −0.09 ms and standard deviation of ∼0.36 ms. For a 600 km radius, the mean and standard deviations are found, respectively, to be −0.32 ms and ∼0.76 ms. Figure 6 shows that the observed distribution is wider than that which would be expected due to geometry. The error in both VLF and TGF measurements are conservatively taken to be uniform 1 ms windows. TGF times on RHESSI are specified with 1 ms precision. Although Palmer measurements are synchronized with 200 ns GPS signals, small errors result from visual estimation of the sferic start time, and due to the sferic group velocity taken to be c. Subtracting the variance due to geometry and measurement error yields a remainder variance of σ_{REM} = 2.2 ms.

[18] Separate and independent of that, however, is the overall mean of +0.88 ms, generally in agreement with results from *Cummer et al.* [2005]. This nominally suggests that TGFs may precede lightning. However, identical analysis of TGFs from the BATSE instrument (Cohen et al., submitted manuscript, 2006) finds the mean sferic arrival to be −2.5 ms, indicating that TGFs occur after associated lightning. By comparison of those results with these using the small sample t-test, *Cohen et al.* [2006] determines that, to 90% confidence, the absolute difference between the RHESSI clock and BATSE clock is between 1.3 and 5.4 ms. At this time, it is not possible to determine absolute timing with the RHESSI instrument to better than 2−3 ms, as comparisons to other spacecraft data have shown [*Stanley et al.*, 2006], while BATSE timing is accurate to 0.1 ms.

[19] Although RHESSI's detectors are not sizable enough to capture a large number of photons for each event, the brightness (peak photon count), duration and mean energy are recorded for each event. Scatter plots (not shown) compare those to ELF/VLF properties (VLF and ELF intensity percentile, arrival time and azimuth relative to time zero and RHESSI-azimuth) for the associated sferics. No evidence is found of a correlation between any of the VLF and the TGF properties.

4. Conclusions

[20] The majority of TGF events (76%) occur in association with lightning discharges occurring in the RHESSI footprint region, within a few ms of the TGF. The remaining TGFs are clearly not associated with any radio atmospheric, and thus by implication occur without any accompanying CG lightning discharge below 3 kA, and may possibly not be accompanied by any lightning discharge. The peak VLF intensity of the lightning discharges associated with TGFs are often among the most intense among those from the same storm. This tendency toward peak-VLF intensity varies by region, and appears stronger for oceanic regions. However, the time-integrated ELF energy of the associated sferics exhibits no such tendency, in agreement with *Cummer et al.* [2005]. Statistical analysis of the spread in arrival time suggests a ∼2 ms variance in the sferic arrival time due to factors other than geometry and measurement error, possibly representing variances due to the underlying physical mechanism(s) of TGF production.

[21] **Acknowledgments.** This work was supported by the NSF under grant OPP-0233955 to Stanford University. RHESSI was supported by NASA under grant NAS5-98033.

References

Cohen, M. B., et al. (2006), Terrestrial gamma ray flashes observed on BATSE/CGRO and ELF/VLF radio atmospherics, *J. Geophys. Res.*, doi:10.1029/2005JD006987, in press.

Cummer, S. A., and U. S. Inan (1997), Measurement of charge transfer in sprite-producing lightning using ELF radio atmospherics, *Geophys. Res. Lett.*, *24*(14), 1731−1734.

Cummer, S. A., Y. Zhai, W. Hu, D. M. Smith, L. I. Lopez, and M. A. Stanley (2005), Measurements and implications of the relationship between lightning and terrestrial gamma ray flashes, *Geophys. Res. Lett.*, *32*, L08811, doi:10.1029/2005GL022778.

Cummins, K. L., et al. (1998), A combined TOA/MDF technology upgrade of the U.S. National Lightning Detection Network, *J. Geophys. Res.*, *103*, 9035−9044.

Davies, K. (1990), *Ionospheric Radio*, Perefrinus, London.

Fishman, G. J., et al. (1994), Discovery of intense gamma-ray flashes of atmospheric origin, *Science*, *264*, 1313.

Gurevich, A., Y. Medvedev, and K. Zybin (2004), New type discharge generated in thunderclouds by joint action of runaway breakdown and

extensive atmospheric shower, *Phys. Lett. A*, *329*, 348–361, doi:10.1016/j.physleta.2004.06.099.

Inan, U. S., and N. G. Lehtinen (2005), Production of terrestrial gamma-ray flashes by an electromagnetic pulse from a lightning return stroke, *Geophys. Res. Lett.*, *32*, L19818, doi:10.1029/2005GL023702.

Inan, U. S., S. C. Reising, G. J. Fishman, and J. M. Horack (1996), On the association of terrestrial gamma-ray bursts with lightning and implications for sprites, *Geophys. Res. Lett.*, *23*(9), 1017–1020.

Lehtinen, N. G., T. F. Bell, and U. S. Inan (1999), Monte Carlo simulation of runaway MeV electron breakdown with application to red sprites and terrestrial gamma ray flashes, *J. Geophys. Res.*, *104*, 24,699–24,712.

Lehtinen, N. G., U. S. Inan, and T. F. Bell (2001), Effects of thunderstorm-driven runaway electrons in the conjugate hemisphere: Purple sprites, ionization enhancements, and gamma rays, *J. Geophys. Res.*, *106*, 28,841–28,856.

Reising, S. C., U. S. Inan, T. F. Bell, and W. A. Lyons (1996), Evidence for continuing currents in sprite-producing cloud-to-ground lightning, *Geophys. Res. Lett.*, *23*(24), 3639–3642.

Roussel-Dupr, R., E. Symbalisty, Y. Taranenko, and V. Yukhimuk (1998), Simulations of high-altitude discharges initiated by runaway breakdown, *J. Atmos. Sol. Terr. Phys.*, *60*(7–9), 917–940.

Smith, D. M., L. I. Lopez, R. P. Lin, and C. P. Barrington-Leigh (2005), Terrestrial gamma-ray flashes observed up to 20 MeV, *Science*, *307*, 1085.

Stanley, M. A., X.-M. Shao, D. M. Smith, L. I. Lopez, M. B. Pongratz, J. D. Harlin, M. Stock, and A. Regan (2006), A link between terrestrial gamma-ray flashes and intracloud lightning discharges, *Geophys. Res. Lett.*, *33*, L06803, doi:10.1029/2005GL025537.

Uman, M. (1987), *The Lightning Discharge*, Elsevier, New York.

Westerlung, S., and F. H. Reder (1973), VLF propagation at auroral latitudes, *J. Atmos. Terr. Phys.*, *35*, 1453.

Wood, T. G. (2005), Geo-location of individual lightning discharges using implulsive VLF electromagnetic waveforms, Ph.D. thesis, Stanford Univ., Stanford, Calif.

Wood, T. G., and U. S. Inan (2004), Localization of individual lightning discharges via directional and temporal triangulation of sferic measurements at two distant sites, *J. Geophys. Res.*, *109*, D21109, doi:10.1029/2004JD005204.

M. B. Cohen, U. S. Inan, and R. K. Said, STAR Laboratory, Electrical Engineering Department, Stanford University, 350 Serra Mall Room 356, Stanford, CA 94305, USA. (inan@stanford.edu)

L. I. Lopez, Department of Physics and Astronomy, San Francisco State University, 1600 Holloway, San Francisco, CA 94132-4163, USA.

D. M. Smith, Santa Cruz Institute of Particle Physics, University of California, Santa Cruz, 1156 High Street, Santa Cruz, CA 95064, USA.